An infinite stiffness aerostatic pad with a diaphragm valve

(Article begins on next page)

19 April 2024

An Infinite Stiffness Aerostatic Pad with a Diaphragm Valve

Danial Ghodsiyeh[1], Federico Colombo[1], Luigi Lentini[1*], Terenziano Raparelli[1], Andrea Trivella[1], Vladimir Viktorov[1]
[1]Department of Mechanical and Aerospace Engineering, Politecnico di Torino,
Turin, Corso Duca degli Abruzzi 24, 10129
*Corresponding Author: luigi.lentini@polito.it

Abstract:

This work presents a prototype of a compensated aerostatic pad which consists in the integration of a commercial pad with a custom-built regulating pneumatic valve. The performance of the system is studied both in static and transient conditions. The stability and the capacity of compensation of the protype are proved performing step force tests. Moreover, the paper describes the lumped parameter model of the compensated pad. To take into account the compensating action of the valve, a distinctive numerical procedure was developed. Experimental and numerical results are in good agreement and demonstrate that once a suitable initial set-up is defined, the integrated regulating valve allows bearings with quasi-static infinite stiffness to be obtained.

Nomenclature

A	Pad length [m]
B	Pad depth [m]
C_1	Conductance of the valve nozzle [kg/(s·Pa)]
C_2	Conductance of the pad orifice [kg/(s·Pa)]
F_p	Load capacity of the pad [N]
G_1	Air flow rate through the valve nozzle [kg/s]
G_2	Air flow rate through the pad orifice[kg/s]
G_3	Air flow rate through the air gap [kg/s]
K_T	Square root of the ratio between the valve and a reference absolute temperature [-]
L	Function correlates the orifice outlet pressure and the mean air gap pressure
P_0	Mean air gap pressure [Pa]
P_1	Valve pressure [Pa]
P_2	Outlet pressure at the pad orifice [Pa]
P_a	Ambient Pressure [Pa]

P_S Supply Pressure [Pa]

Q Air flow rate of the pad [l/min ANR 20°C]

R Air constant [J/(kg·K)]

R_1 Pneumatic resistance of the valve nozzle [(s·Pa)/kg]

R_2 Pneumatic resistance of the pad orifice [(s·Pa)/kg]

R_3 Pneumatic resistance of the air gap [(s·Pa)/kg]

Re_a Reynolds number of the pad orifice [-]

Re_v Reynolds number of the valve nozzle [-]

T Absolute temperature [K]

V_0 Air gap volume [m³]

V_1 Volume of the valve chamber [m³]

V_2 Sum of the air gap and the grooves volumes [m³]

V_g Grooves volume [m³]

a Length of the grooved supply line [m]

b Depth of the grooved supply line [m]

b_c Theoretical critical pressure ratio [-]

d_m Diameter of the valve membrane [m]

d_n Diameter of the valve nozzle [m]

d_p Diameter of the pad orifice [m]

err_F Convergence error related to the load capacity [-]

err_G Convergence error related to the air mass flow rate [-]

k_m Stiffness of the valve membrane [N/m]

h Air gap height [m]

h_{eqv} Equivalent air gap height considering the presence of grooves [m]

h_g Grooves depth [m]

s Membrane thickness [m]

t Time [s]

Δt Time step of the model [s]

w_g Groove width [m]

x Membrane-Nozzle distance [m]

$x_{by-pass}$	By-pass distance [m]
x_n	Initial membrane-nozzle distance [m]
x_v	Membrane deflection [m]
μ	Dynamic viscosity [Ns/m^2]

1. Introduction

Because of their low friction, long life and cleanness, air pads are widely used in all applications requiring high positioning accuracy, e.g., coordinate measuring machines (CMM) and linear guides of tool machines [1]. However, this kind of bearings suffer from relative low stiffness and poor damping. In this regard, different solutions have been proposed to improve aerostatic pad performance. The more straightforward approach is to design different types of feeding systems to increase their inherent capacity of compensation [2,3]. Many experimental and numerical analyses have proposed optimization strategies to increase the characteristics of air pads by modifying the type, size, number and location of their restrictors [4–7]. However, these approaches lead only to limited global performance enhancements. Machining shallow grooves [8–10] on the active surface of the pad makes it possible to increase the stiffness of the pads but may reduce their damping and compromise their dynamic stability. The best results are obtained by replacing simple or pocketed orifices with porous restrictors. Porous bearings are characterized by smoother air gap pressure distribution, higher stiffness, damping and load capacities [11]. Despite their higher performance, this kind of bearing presents some drawbacks related to the porous material adopted and its manufacturing. These materials should be characterized by suitable permeabilities (lower than 10^{-12}m^2 [3]) and mechanical properties [12–14].

Conversely, passive and active compensation methods represent a more effective solution to obtain bearings with higher performance [15]. These methods consist in enhancing the bearing

performance through the integration of pads with additional elements or devices. Passive compensation methods use components which require only the energy associated with the supply pressure of the bearing, e.g., pneumatic valves and compliant elements. By contrast, actively compensated bearings are equipped with elements such as sensors, controllers and actuators that require external sources of energy to function. Because of their high dynamics, piezoelectric actuators are extensively used. Colombo et al. [16] proposed an actively compensated aerostatic bearing employing a geometrical compensation method. A piezoelectric stack actuator, controlled by a PI controller, is used to suitably modify the thickness of active pad to compensate for air gap variations. Similarly, Al Bender [17] and Aguirre [18] proposed an active circular air pad with a variable gap geometry. Santos et al. [19–22] along with Mizumoto et. al [23] developed similar active compensation solutions where the stroke of piezoelectric actuators controls the air mass flow rate exhausted from each bearing restrictor.

Despite their higher performance, active compensation solutions are still too expensive to be employed in current industrial applications. Conversely, passive compensation solutions represent a valid and cheaper alternative, notwithstanding their lower bandwidth. Passive compensation methods usually exploit the compliance of elastic elements or pneumatic valves to improve bearing behaviours. Newgard et al. [24] proposed the use of elastic orifices. The deformation of these elastic inserts makes it possible to suitably compensate for load variations, thus increasing the stiffness of the bearing.

Blondeel et al.[25], Snoeys [26] and Bryant [27] present a prototype of compensated bearing with convergent gap geometry. It consists in using a compliant structure as active surface of the pad. It was found that a suitable selection of the geometry of the compliant surface makes it possible to

optimize the air pad stiffness. Chen and Lin [28] proposed a grooved aerostatic bearing with a disk-spring compensator to increase the bearing damping.

Despite their simple construction, ease of integration and relatively low cost, pneumatic valves have been seldom employed to increase aerostatic pad performance. This paper presents a study on the functioning and performance of a compensation solution employing a diaphragm valve. Starting from the preliminary results obtained in [29], this work details the use of this kind of compensation method. Differently from [29], the structure of the valve was modified to experimentally evaluate the deflection of the diaphragm of the valve during its functioning. Moreover, the performance of the compensated pad was assessed through a new and improved static test bench and a step force test bench. Regarding the system modelling, previous lumped parameter models [30,31] were suitably modified and used to predict the behavior of the proposed compensated pad. This model was developed using a distinctive iterative procedure to take into account the compensating action of the employed pneumatic valve. Experimental and numerical tests demonstrate that the effectiveness of the proposed solution mainly depends on the diaphragm stiffness and its initial distance from the nozzle of the valve. It was shown that, once an optimal initial set-up is defined, the integrated valve makes it is possible to obtain bearings with quasi-static infinite stiffness. The last part of the work numerically and experimentally demonstrates the stability of the pad through step force tests.

2. Materials and Methods
2.1. The proposed solution

Figure 1 shows a photograph of the proposed compensation solution. It consists in the integration of a commercial aerostatic pad and a custom-built diaphragm valve.
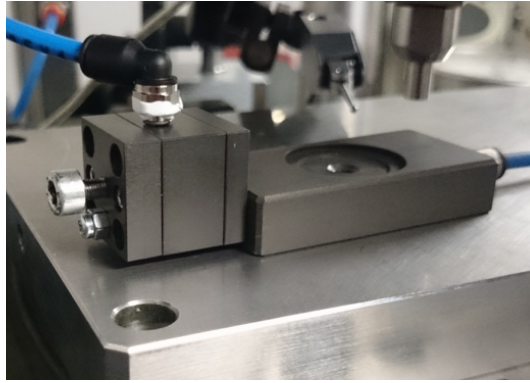
Figure 1: Photograph of the proposed compensation solution

Figures 2a and 2b shows a cross section of the valve and the main geometrical details of the commercial pad. The diaphragm valve consists of a compliant chamber, a nozzle, a regulating screw, a Bellville spring and several O-rings. The chamber of the valve is supplied through a nozzle of diameter d_n= 0.5 mm. Once pressurized, the volume of the chamber increases depending on the deflection of a metallic membrane with a diameter (d_m) of 6 mm and a thickness (s) 0.08 mm. The initial distance between the nozzle and the membrane (x_n) can be manually adjusted through the regulating screw. The Bellville washer is necessary to preload the regulating screw thus increasing the accuracy of the nozzle positioning.
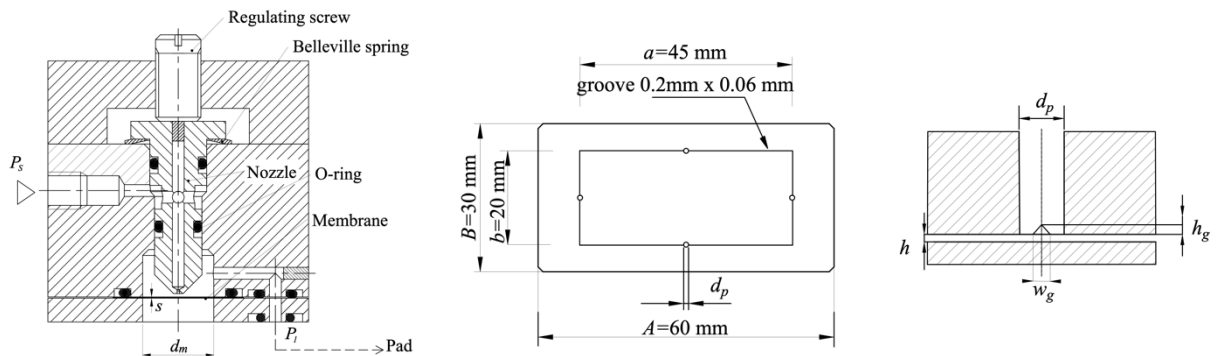
In this instance, the valve supplies an air pad with a rectangular base (AxB) of 60x30 mm² and four simple orifices with a diameter d_p= 1 mm. Each restrictor is located in the middle of each side of a grooved rectangular supply line with a base (a) of 45 mm and a depth (b) of 20 mm. The grooves present a triangular cross-section with a base (w_g) of 0.2 mm and a height (h_g) of 0.06 mm.

2.2. **The model of the proposed system**

2.2.1. **Model description**

Figures 3a and 3b show a functional and a pneumatic scheme of the proposed system.
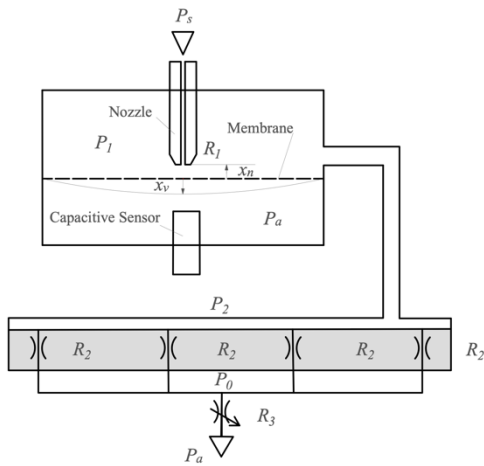
Figure 3a: Functional scheme of the proposed compensation solution
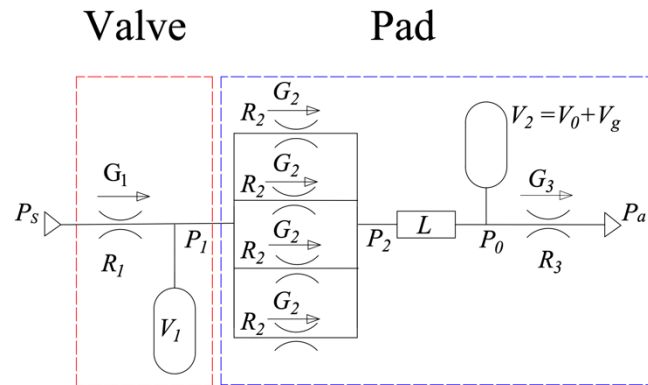

Figure 3b: Pneumatic scheme of the proposed compensation solution

As can be seen in Figure 3, the system is modelled as a pneumatic circuit composed of lumped resistances and volumes. Starting from the upstream, the volume of the valve ($V_1 = 1.2 \cdot 10^{-7} m^3$) is supplied with a constant pressure (P_s) through the nozzle. The value of the air mass flow rate

supplied by the nozzle (R_1) depends on its initial position (x_n), the deflection of the membrane (x_v), the supply pressure (P_s) and the pressure inside the valve chamber (P_1). Designating the membrane stiffness as $k_m = 1.8 \cdot 10^5$ N/m, its distance from the nozzle can be obtained as follows:

$$x = x_n + \overbrace{\frac{\pi d_m{}^2}{4} \frac{(P_1 - P_a)}{k_m}}^{x_v} \tag{1}$$

It should be noted that setting negative values of x_n (in the absence of the supply pressure P_s) implies an initial preload of the membrane. Differently from the previous investigations [29], to measure the membrane deflection a displacement capacitive sensor was embedded into the structure of the valve (see Figure 3a). This made it possible to experimentally measure the membrane deflection during tests. Through this improved experimental set-up, it was found that the valve works in different ways depending of the nozzle-membrane distance x. In fact, when the membrane is initially preloaded ($x_n < 0$) and the pad is lightly loaded (this corresponds to a low value of P_1), the valve membrane exhibits a higher stiffness. Once the pressure P_1 is high enough to overcome the preload pressure, the stiffness of the membrane changes and remains almost constant over the remaining operating range. This phenomenon is modelled by introducing the following by-pass condition:

$$\begin{cases} x = 12 \ \mu m; & x \leq 12 \ \mu m \\ x = x_n + \dfrac{\pi d_m{}^2}{4} \dfrac{(P_1 - P_a)}{k_m}; & x > 12 \mu m \end{cases} \tag{2}$$

The air mass flow rate passing through the nozzle is computed by means of the ISO formula 6358 [32]:

$$G_1 = K_T\, C_1 P_s\, \sqrt{1 - \left(\frac{\frac{P_1}{P_S} - b_c}{1 - b_c}\right)^2} \qquad (3)$$

where, K_T is the square root of the ratio between the valve (293 K) and a reference absolute temperatures (273 K), b_c is the theoretical critical pressure ratio (0.528), P_1 is the pressure inside the chamber of the valve and C_1 is the conductance of the nozzle [33]:

$$C_1 = 1.05(1 - 0.3\, e^{-0.005\, Re_v})\, \frac{0.685}{\sqrt{R\,T}}\, \pi\, d_n\, x \qquad (4)$$

Re_v is the Reynolds number related to the air mass flow rate passing through the nozzle which is computed as:

$$Re_v = \frac{G_1}{\pi \mu d_n} \qquad (5)$$

Similarly, the air mass flow rate passing through the orifices of the pad (R_2), its conductance and the related Reynolds number are computed as:

$$G_2 = K_T\, C_2 P_1\, \sqrt{1 - \left(\frac{\frac{P_2}{P_1} - b_c}{1 - b_c}\right)^2} \qquad (6)$$

$$C_2 = 1.05(1 - 0.3\, e^{-0.005\, Re_a})\, \frac{0.685}{\sqrt{R\,T}}\, (\pi\, d_p\, h + w_g\, h_g) \qquad (7)$$

$$Re_a = \frac{G_2\, h}{\mu(\pi d_p h + w_g\; h_g)} \tag{8}$$

Here, the presence of the grooves is taken into account by considering an equivalent area $A_{eqv} = \pi\, d_p\, h + w_g\, h_g$ in Equation 7 and an equivalent air gap height $h_{eqv} = \frac{\pi d_p h + w_g\; h_g}{\pi d_p}$ in Equation 8 [34]. The laminar mass flow rate exhausted through the air gap (R_3) is evaluated by the integration of the Reynolds equations along each side of the pad and the resulting expression is the following:

$$G_3 = \frac{1}{6\mu RT}\left(\frac{b}{A-a} + \frac{a}{B-b}\right)(P_0^2 - P_a^2)h^3 \tag{9}$$

where, P_0 is considered as the mean constant pressure inside the area of the grooved rectangular supply line. The expression of this pressure is computed through a semi-empirical formula [31] which correlates P_0 and P_2 through the function L (see Figure 3b):

$$P_0 = \left[1 - 0.14^{\left(\frac{5}{h}\right)}\right](P_2 - P_a) + P_a \tag{10}$$

where, h is the air gap height expressed in μm. The pressure inside the valve P_1 and the pressure at the outlet of each restrictor P_2 are computed by considering the continuity equations of the related volumes V_1 and $V_2 = V_0 + V_g$.

$$G_1 - 4G_2 = \frac{V_1}{RT}\frac{dP_1}{dt} \tag{11}$$

$$4G_2 - G_3 = \frac{1}{RT}\left(P_0\frac{dV_2}{dt} + V_2\frac{dP_0}{dt}\right) \tag{12}$$

The load carrying capacity of the pad is computed by assuming that the surface of the pad is perfectly smooth and that the pressure distribution outside the rectangular area surrounded by the grooves is linear:

$$F_p = \left[ab + AB + \frac{(Ab + aB)}{2} \right] \frac{(P_0 - P_a)}{3} \tag{13}$$

2.2.2. The Iterative Procedure

The lumped model of the system is implemented in Matlab using the Euler explicit method and simulating the filling of the system volumes. The filling of the volumes was simulated by iteratively solving the time dependent Reynolds equation assuming a time step (Δt) of 10^{-7} s. Since the compensating action of the valve renders the load capacity F_p and the air mass flow rate G non-injective functions of the air gap height h (there are more than one load capacities and air mass flow rates for the same air gap height value), a specific numerical procedure was developed. This procedure consists of two main parts and the related flow charts are shown in Figures 4. The first part (see Figure 4a) is necessary to compute a initial static solution of the problem (F_{p_0}, G_0, P_{0_0} P_{1_0}, and P_{2_0}) [35]. The load capacity F_{p_0} and the air mass flow rate G_0 of the pad are computed by considering the air gap height h_0 as an input parameter of the model. Once the convergence conditions are simultaneously satisfied (Equations 14):

$$err_F = \frac{F_p{}^t - F_p{}^{t-1}}{F^t} < 10^{-12}$$

$$err_G = \frac{G_1{}^t - G_1{}^{t-1}}{G^t} < 10^{-12} \tag{14}$$

the load capacity F_{p_0}, air mass flow rate G_0, and the pressures P_{0_0}, P_{1_0} and P_{2_0} are used as input variables in the second main part of the code along with the initial input parameters. In this second step, h_0, F_{p_0}, G_0, P_{0_0}, P_{1_0}, P_{2_0} define the initial static condition of the problem. Starting from this initial condition, the air gap values that guarantee the equilibrium of the pad are iteratively computed by simulating the application of a step force ΔF (in the time domain). Given the initial static condition (h_0, F_{p_0}, G_0, P_{0_0}, P_{1_0}, P_{2_0}) and the selected step force ΔF, the external load F^{ext} acting on the pad is computed as:

$$F^{ext}{}_i = F_{p_0} + i \cdot \Delta F \qquad (15)$$

where, i is the number of iterative steps that have been already solved ($i = 0, 1, 2, \dots, i_{max}$). In each iterative step (i), the equilibrium air gap height is computed by solving the equilibrium equation of the pad (equation 16) through Euler's explicit method:

$$F^{ext} = F_p - M\ddot{h} \qquad (16)$$

where, M is the moving mass of the pad. Once the equilibrium is reached ($M\ddot{h} \approx 0$ and the convergence conditions are satisfied), the obtained results are used as new initial condition and the new external load F^{ext} is obtained from the previous one by adding a further step force ΔF (see equation 15). It should be noted that the discretisation and the range of the obtained characteristic curves of the pad depends on the selected step force ΔF and the number of step force simulated i_{max}. By comparing the flow charts related to the two part of the described algorithm, it is observable that they differ by the selection of the input parameters (h rather than F_p) but present a similar structures consisting in defining the input parameter, initialising variables and solving the governing equations until the defined convergence conditions (Equations 14) are satisfied.

Figure 4a

START

INPUT-PARAMETERS:
- Geometry: d_p, h_g, w_g, A, a, B, b, d_m, d_n
- Time step: Δt
- Fluid: T, μ, R
- Set-up: P_s, $x_{by-pass}$, x_n, h

VARIABLE INIZIALISATION:
- Pressures: P_1, P_2, P_0
- Reynolds' no.: Re_v, Re_a
- Air Flow: G_1, G_2, G_3
- Load capacity: F_p

COMPUTATION:
- Pressures: P_1, P_2, P_0
- Mem.-Noz. Distance: x
- Reynolds' no.: Re_v, Re_a
- Air Flow: G_1, G_2, G_3
- Load capacity: F_p

errF$> 10^{-12}$ & errG$> 10^{-12}$ — Y

N

OUTPUT PARAMETERS:
- Load Capacity: F_{p0}
- Pressures: P_{10}, P_{20}, P_{00}
- Air Flow: G_0
- Air Gap: h_0
- Nozzle Position: x_n

END

Figure 4b

START

INPUT-PARAMETERS:
- Load Capacity: F_{p0}
- Pressures: P_{10}, P_{20}, P_{00}
- Air Flow: G_0
- Air Gap: h_0
- Nozzle Position: x_n
- Time step: Δt
- $i=0$

VARIABLE INITIALISATION
- Applied Load: $F_{p0}+ i\,\Delta F$
- $i=i+1$

COMPUTATION:
- Pressures: P_1, P_2, P_0
- Mem.-Noz. distance: x
- Reynolds' no.: Re_v, Re_a
- Air Flow: G_1, G_2, G_3
- Air gap height: h

errF$> 10^{-12}$ & errG$> 10^{-12}$ — Y

N

$i=i_{max}$ — N

Y

OUTPUT PARAMETERS:
- Load Capacity: F_p
- Pressures: P_1, P_2, P_0
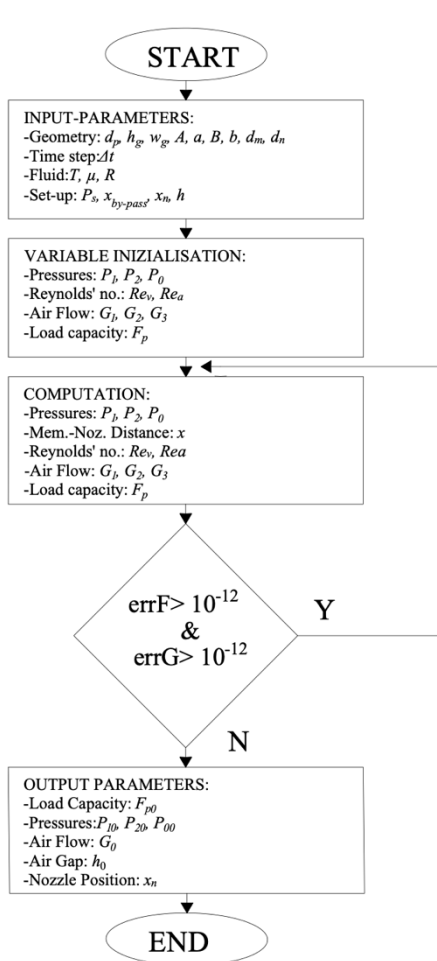- Air Flow: G
- Air Gap: h
- Mem.-Noz. Distance: x

END

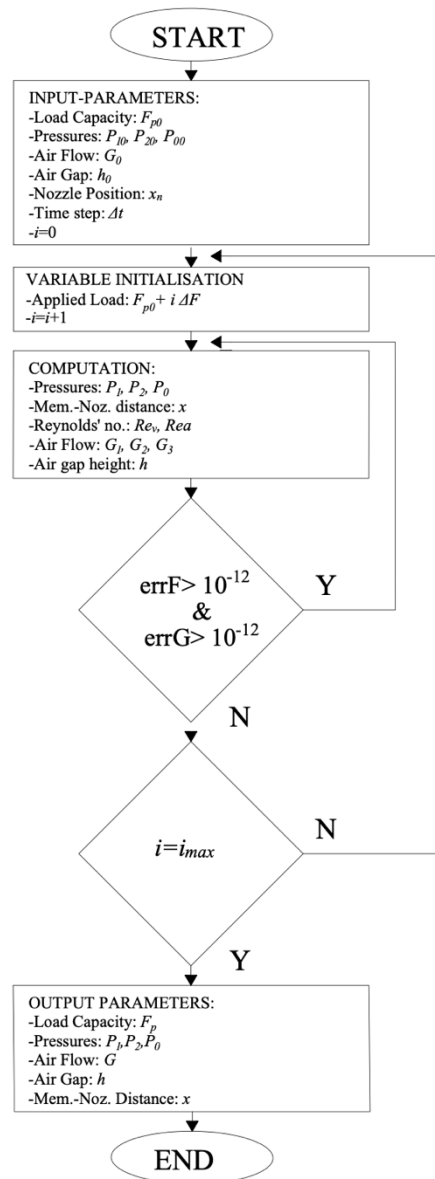Figure 4a: First iterative procedure of the proposed model (Initial Static Solution)

Figure 4b: Second iterative procedure of the proposed model (Static Characteristic curves)

2.2.3. Infinite stiffness and overcompensation

This section briefly explains the effect of the valve regulation on the stiffness of the compensated pad. Depending on the operating conditions and initial set-up, the valve can compensate for air

gap variations leading to positive, negative or infinite static stiffnesses. The effect of the compensating action of the valve on the stiffness can be explained through by linearizing the equations of the model. Starting from an initial working condition (h_0, F_{p_0}, G_0, P_{1_0}, x_0), the external force on the pad is assumed to be increased: $F' = F_0 + \Delta F$. Due to this variation of the external force, a new operating air gap height h', valve pressure P_1' and membrane-nozzle distance x' are established:

$$h' = h_0 + \Delta h$$
$$P_1' = P_{10} + \Delta P_1 \tag{17}$$
$$x' = x_0 + \Delta x$$

Since they depend on the valve pressure P_1 and the air gap height h , the new air consumption $G'=G'(P_1, h)$ and load capacity $F'=F'(P_1, h)$ of the pad are:

$$G' = G_0 + \frac{\partial G}{\partial h}\Delta h + \frac{\partial G}{\partial P_1}\Delta P_1 \tag{18}$$

$$F' = F_0 + \frac{\partial F}{\partial h}\Delta h + \frac{\partial F}{\partial P_1}\Delta P_1 \tag{19}$$

Similarly, the new flow through the valve $G_1'=G_1'(P_1, \Delta x)$ and the new nozzle-membrane distance $x'=x'(P_1)$ are:

$$G_1' = G_0 + \frac{\partial G_1}{\partial P_1}\Delta P_1 + \frac{\partial G_1}{\partial x}\Delta x \tag{20}$$

$$x' = x_0 + \frac{\partial x}{\partial P_1}\Delta P_1 = x_0 + \frac{\pi d_m^2}{4}\frac{1}{k_m}\Delta P_1 \tag{21}$$

The aim of this analysis is to evaluate the new slope of the load vs air gap curve (static conditions) by considering the effect of the valve regulation. To do this, a force variation ΔF is imposed and the correspondent air gap variation Δh is computed. As valve and pad are in series, in the new operating point it is $G' = G_1'$:

$$\frac{\partial G}{\partial h}\Delta h + \frac{\partial G}{\partial P_1}\Delta P_1 = \frac{\partial G_1}{\partial P_1}\Delta P_1 + \frac{\partial G_1}{\partial x}\Delta x \tag{22}$$

The governing equations of the problem can be obtained by combining equations 19, 21 and 22

$$\begin{bmatrix} \dfrac{\partial F}{\partial h} & \dfrac{\partial F}{\partial P_1} \\ \dfrac{\partial G}{\partial h} & \dfrac{\partial G}{\partial P_1} - \dfrac{\partial G_1}{\partial P_1} - \dfrac{\partial G_1}{\partial x}\dfrac{\pi d_m^2}{4}\dfrac{1}{k_m} \end{bmatrix}\begin{pmatrix} \Delta h \\ \Delta P_1 \end{pmatrix} = \begin{pmatrix} \Delta F \\ 0 \end{pmatrix} \tag{23}$$

from which the static stiffness of the active pad can be computed as:

$$-\frac{\Delta F}{\Delta h} = -\frac{\partial F}{\partial h} + \frac{\partial F}{\partial P_1}\frac{\dfrac{\partial G}{\partial h}}{\dfrac{\partial G}{\partial P_1} - \dfrac{\partial G_1}{\partial P_1} - \dfrac{\partial G_1}{\partial x}\dfrac{\pi d_m^2}{4}\dfrac{1}{k_m}} \tag{24}$$

It is clear that the resulting stiffness during the valve regulation is the sum of two contributions: the first one is the stiffness of the not compensated pad, whereas the second one is due to the valve regulation, which causes a variation of P_1 and x.

For example, the stiffness of the passive pad at h=12 μm is $-\frac{\partial F}{\partial h}$ =15.8 N/μm. By considering x=30 μm and P_1=0.45 MPa the following partial derivatives can be calculated:

$$\frac{\partial F}{\partial P_1} = 6.61 \cdot 10^{-4} \text{ N/Pa}$$

$$\frac{\partial G}{\partial h} = 1.25 \cdot 10^{-5} \text{ kg/(s} \cdot \mu\text{m)}$$

$$\frac{\partial G}{\partial P_1} = 3.15 \cdot 10^{-10} \text{ kg/(s} \cdot \text{Pa)}$$

$$\frac{\partial G_1}{\partial P_1} = -2.42 \cdot 10^{-10} \text{ kg/(s} \cdot \text{Pa)}$$

$$\frac{\partial G_1}{\partial x} = 1.466 \text{ kg/(s} \cdot \text{m)}$$

and the stiffness during valve regulation results to be $-\frac{\Delta F}{\Delta h}$ =41.1 N/μm. In this case, it is about

three times the stiffness of the not compensated pad, supplied at pressure P_1. The effect of the

valve regulation mainly depends on the denominator of the second term $\left(\frac{\partial G}{\partial P_1} - \frac{\partial G_1}{\partial P_1} - \frac{\partial G_1}{\partial x} \frac{\pi d_m^2}{4} \frac{1}{k_m} \right)$.

The stiffness of the pad approaches to infinity as this denominator tends to zero. Conversely, when

it is negative and the second terms is higher than the first one, the pad will be overcompensated

(negative stiffness). Moreover, it is evident that the smaller is the membrane stiffness, the more

important is the valve compensation.

2.3. The experimental set up

A static and a step force test bench were employed to assess the static and transient performance

of the proposed solution. Every test was performed with a supply pressure (P_s) of 0.525 MPa

(absolute).

2.3.1. Static test Bench

Figure 5 shows a scheme of the experimental configuration employed for the static characterisations.
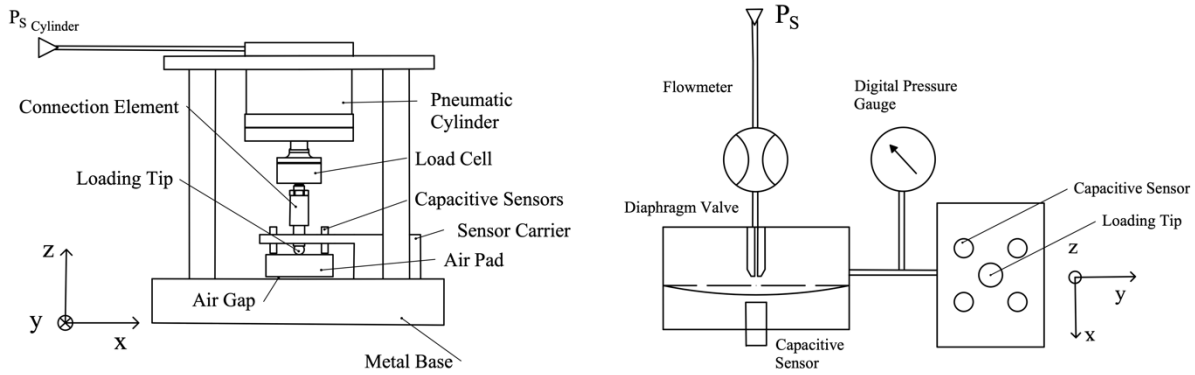

Figure 5: Scheme of the static test bench

The static test bench consists of a metal base, a sensors carrier, a pneumatic cylinder, a load cell and a loading tip. Once the pad under test was located in the centre of the base, varying the supply pressure of the cylinder ($P_{S_{Cylinder}}$) made it possible to modify the external load applied to the pad. This load was transmitted through a mechanical chain composed of the load cell, a connection element and the loading tip. Four capacitive sensors mounted on a sensor carrier were used to measure the pad displacement. The air gap height was evaluated as the difference between the pad positions with and without supply air. Additionally, a flowmeter, a digital pressure gauge and an additional capacitive sensor were used to measure the air flow rate (Q), the pressure inside the valve (P_1) and the membrane deflection (x_v) (see Figure 5b).

2.3.2. Step Force Test Bench

Figures 6a and 6b show a photograph and a scheme of the mechanical configuration of the step force test bench used.
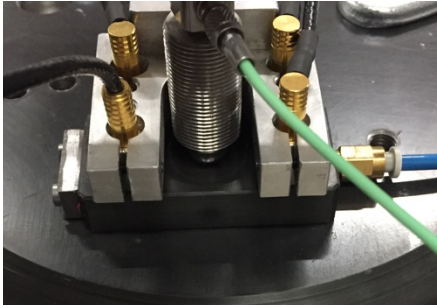
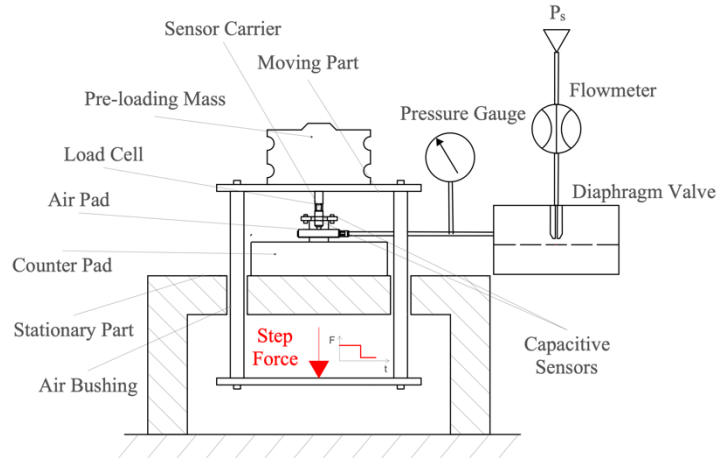Figure 6a: Photograph of the experimental set-up of the step force test bench

Figure 6b: Scheme of the mechanical configuration of the step force test bench

The step force test bench consists of a stationary and a moving part. Two air bushings allow a translational motion between these two parts. The air pad under test was located between the moving part of the test bench and a counterpad. External loads were applied by fixing calibrated masses on the upper part of the moving structure of the test bench. The external force due to these masses was transmitted to the pad through a mechanical chain composed of a load cell and a spherical loading tip. The air gap height of the pad was evaluated via four capacitive sensors as in the previous test bench (see Section 3.3.2). Negative step forces were applied at the bottom of the moving part. An additional weight was bound with a thin rope to the lower crossbeam of the moving part. Negative steps of force were instantaneously generated by cutting the rope. Also in this case, a flowmeter, an additional capacitive sensor and a digital pressure gauge were used to measure the air flow rate (Q), the membrane deflection (x_v) and the valve pressure (P_1).

3. **Results and discussions**
   3.1. **Static Characterisation**

Figures 7, 8 and 9 show the numerical and experimental static curves obtained in the presence of a supply pressure of 0.525 absolute MPa. The effectiveness of the proposed solution was evaluated performing tests with different initial nozzle-membrane distances x_n= 0, -10, -20, -30 μm and comparing these results to those obtained in the absence of the regulating valve.
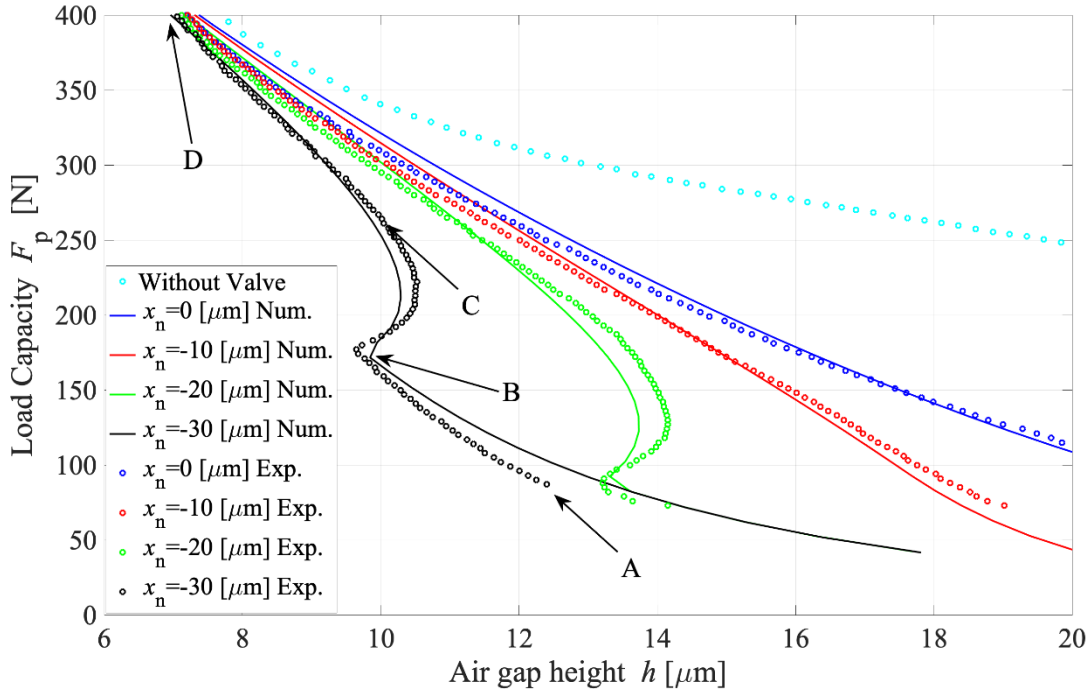

Figure 7: Load capacity curve of the proposed prototype

As it can be seen, the controlled pad exhibits characteristic curves which are significantly different from those of the pad without valve. As in [29], the presence of the valve makes it possible to increase the stiffness and reduce the air consumption of the pad but it diminishes also the load capacity. The valve regulation is evident only for initial nozzle-membrane distances lower that -10 μm. In these instances, starting from higher air gap heights, a by-pass, a regulation and a saturation zone can be identified. The location of these three zones can be clarified looking at the experimental characteristic curves obtained with a membrane-nozzle distance of -30 μm. In the

by-pass region (AB), the valve behaves like a linear pneumatic resistance (see Figure 8). The load applied on the pad generates a pressure P_1 that is not sufficient to create a well-defined clearance between the nozzle and the membrane because of the initial preload imposed on the membrane. Consequently, the air supplied to the pad is due to small air leakages occurring because of local deformations of the membrane that do not allow the complete closure of the valve nozzle. In these instances, the amount of the pressurized air supplied to the pad is computed considering a constant membrane-nozzle distance $x_{by-pass}$ (see equation 2). When the external load increases, the nozzle-membrane distance increases because of the higher valve pressure P_1 and the valve starts regulating (BC). During the regulation, the valve compensates for the air gap variation by increasing the air flow rate supplied to the pad. It is worth pointing out that the amount of air supplied by the valve mainly depends on the stiffness of the valve membrane (k_m) and the initial membrane-nozzle distance (x_n). As discussed in section 2.2.3, if the membrane stiffness is not suitably selected, the effect of the compensation can be poor or excessive (overcompensation).
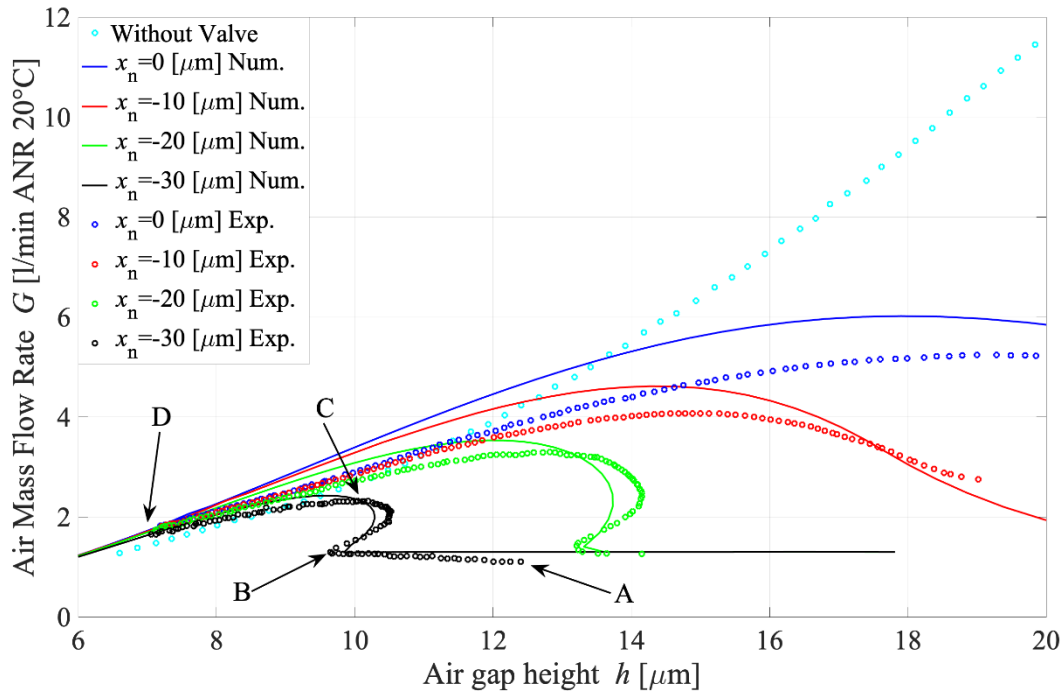
Figure 8: Air consumption curve of the proposed prototype

The valve regulation ends (C) when the nozzle saturates because of its excessive distance from the membrane. This operating condition corresponds to the maximum air consumption of the pad. In the saturation zone (CD), the load and air consumption curves exhibit trends that depend only on the performance of the integrated pad. Figure 7 compares the numerical and experimental load carrying capacity curves of the compensated and not compensated pad. Analysing the regulation zones, it appears that the valve compensation is effective for initial membrane nozzle distances lower than -10 μm. Moreover, the regulation zone moves towards lower air gap height as the initial membrane-nozzle distance is decreased. In this instance, because the valve generates an overcompensation, the pad exhibits negative stiffnesses when x_n=-20 and -30 μm. Regarding the air consumption curves (see Figure 8), decreasing the initial membrane-nozzle distance (x_n) enlarges the by-pass region (AB) and reduces the air consumption of the pad. Figure 9 compares

the numerical and the experimental nozzle-membrane distance expressed as a function of the pressure P_1.
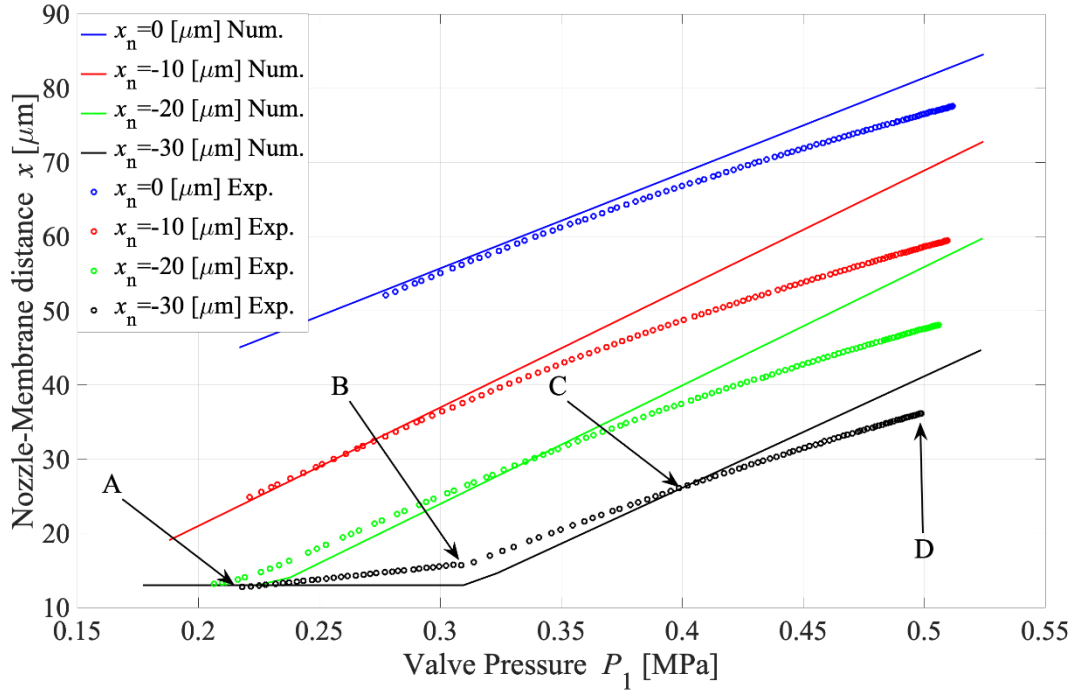

Figure 9: Membrane deflection vs valve pressure

From the curves in Figure 9, it can be seen that the nozzle-membrane displacement increases almost proportionally with the pressure in the valve chamber. In the absence of the regulating action of the valve, the curves present an almost constant slope. Conversely, when the valve compensates for load variations (x_n=-20 and -30 μm), the curves present two different slopes. The by-pass zone (AB) is characterised by a higher stiffness ($8.07 \cdot 10^5$ N/m), whereas in the regulation (BC) and saturation (CD) zones the membrane exhibits a lower and almost constant stiffness ($2.61 \cdot 10^5$ N/m). As mentioned above, this is due to the fact that the air pressure P_1 is not high enough to overcome the preload generated by the nozzle. In view of the experimental results obtained, the numerical model was exploited to study the effect of the membrane stiffness on the

pad performance. These simulations were performed considering membrane stiffnesses of $1.5 \cdot 10^5$, $2 \cdot 10^5$, $2.5 \cdot 10^5$ and $3 \cdot 10^5$ N/m, an initial nozzle-membrane distance of -25 μm and a by-pass distance of 12 μm. These numerical results (see Figures 10a and 10b) demonstrate that it is possible to obtain pad with quasi-static infinite stiffness by performing a suitable tuning of the membrane stiffness. In particular, for this pad, the optimal value of the membrane stiffness is about $3 \cdot 10^5$ N/m. Additionally, it can be seen that increasing the membrane stiffness leads to significant reductions of the air consumption but at the same time reduces the amplitude of the regulation zone.
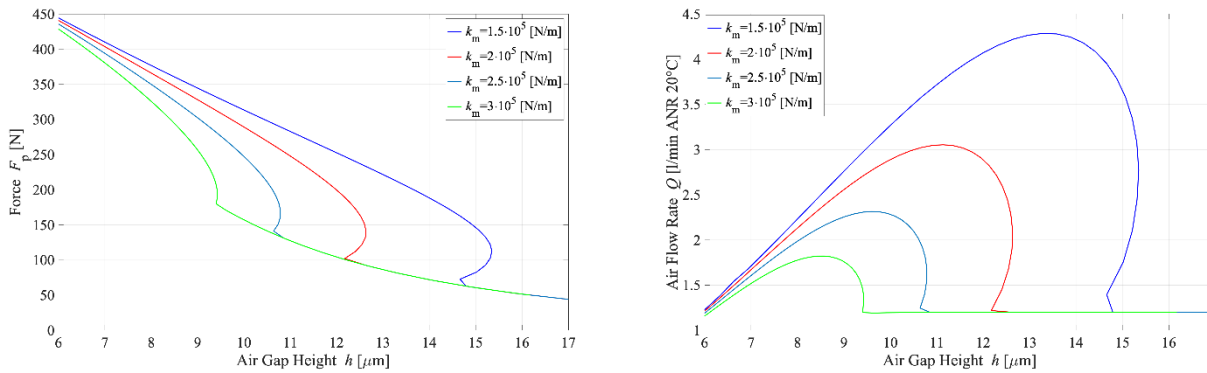
(a) Load Capacity   (b) Air Consumption

Figure 10: The influence of the membrane stiffness on the pad performance.

3.2. **Step force test**

Step force tests (see Section 2.3.2) were performed to evaluate the compensation capacity of the proposed system and to prove the stability of the proposed method even when the pad exhibits negative static stiffnesses. For this reason, the stiffness of the membrane was reduced (k_m=1.15$\cdot 10^5$ N/m) to enlarge the amplitude of the regulation zone exhibiting a negative stiffness. The initial nozzle-membrane distance was equal to -17.5 μm. Before performing the step force

test, the static characterisation of the pad was repeated on the step force test bench (see Figures 11a and 11b). After this, the capacity of compensation was evaluated by imposing negative step of 20 N.
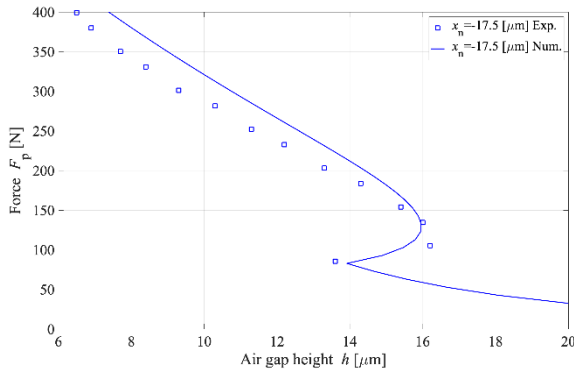

Figure 11a: Load capacity curve of the proposed prototype measured on the step force test bench
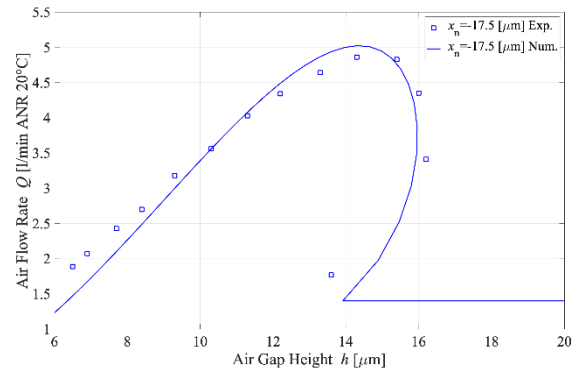

Figure 11b: Air consumption curve of the proposed prototype measured on the step force test bench

Figures 11a and 11b show the numerical and the experimental static curves obtained on the static test bench. As can be seen, compared to the previous curves (see Figure 7 and 8), the regulation zone is larger and the air consumption is higher due to the lower stiffness of the membrane. Figures 12 and 13 compare the numerical and experimental results related to step force tests performed in the regulation when the pad exhibits negative and positive stiffnesses.
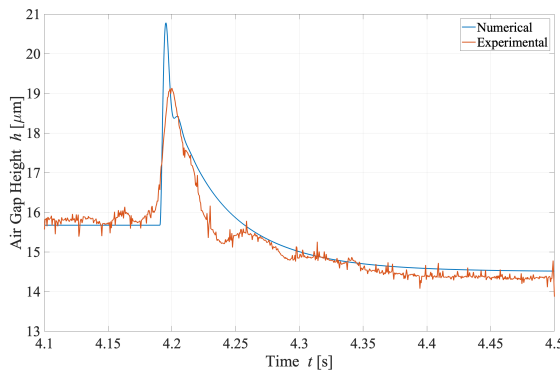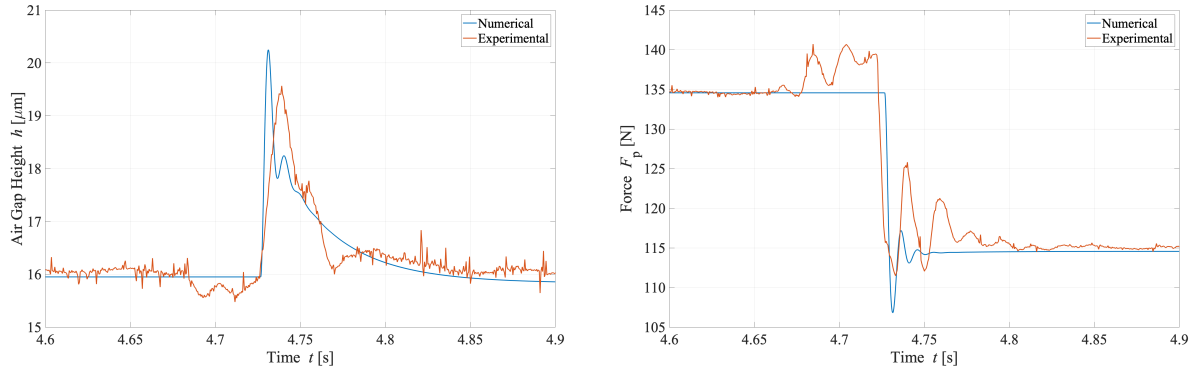

(a) Air Gap Height
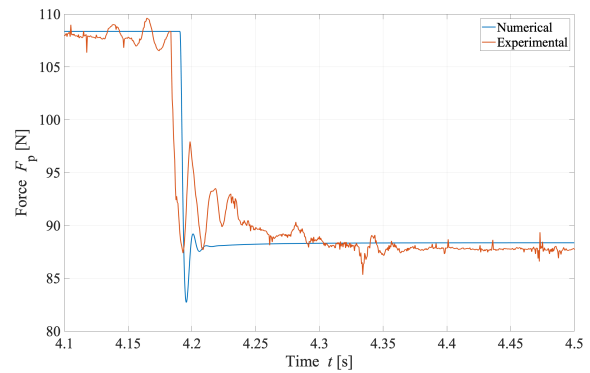
(b) Force

Figure 12: Step force response of the proposed prototype (negative stiffness)

(a) Air Gap Height

(b) Force

Figure 13: Step force response of the proposed prototype (positive stiffness)

As can be observed, the system response is stable in both the considered cases and the settling time of the system varies depending on the considered working condition. To conclude, the step force results along with the numerical results obtained by varying the membrane stiffness demonstrate that when the membrane stiffness is suitably selected, the proposed methodology makes it possible to obtain stable aerostatic pads with quasi-static infinite stiffness.

4. Conclusions

This paper presents a compensation method to increase the stiffness of aerostatic pads.

This method consists in using a custom-built regulating valve to suitably modify the performance of pads. Starting from the preliminary results obtained in [29], the structure of the valve was modified to experimentally evaluated the diaphragm deflection during its functioning. Additionally, the effect of the valve regulation was further investigated considering operating conditions where the proposed method makes it possible to obtain negative and infinite static

stiffnesses. The performance of the proposed solution was investigated performing numerical and experimental tests. Numerical results are in good agreement with the experimental ones. It was found that the effectiveness of the valve regulation mainly depends on the diaphragm stiffness and its initial distance from the nozzle of the valve. Depending on these two parameters the valve compensation can lead to positive, negative or infinite static stiffness. It was demonstrated that the controlled pad exhibits negative stiffnesses because the overcompensation of the valve. This was confirmed by verifying the stability of the system through step force tests. Once verified, the accuracy of the numerical model, it was used to demonstrate that a suitable tuning of the membrane stiffness makes it possible to obtain infinite stiffness over a portion of the characteristic curve of the pad. These results indicate that the proposed method has the potential to become an efficient and cost-effective method to enhance the static performance of aerostatic pads.

5. References

[1]   Lentini, L., Moradi, M., and Colombo, F., 2018, "A Historical Review of Gas Lubrication: From Reynolds to Active Compensations," Tribology in Industry, **40**(2), pp. 165–182.

[2]   Rowe, W. B., 2012, *Hydrostatic, Aerostatic, and Hybrid Bearing Design*, Elsevier.

[3]   Fourka, M., and Bonis, M., 1997, "Comparison between Externally Pressurized Gas Thrust Bearings with Different Orifice and Porous Feeding Systems," Wear, **210**(1–2), pp. 311–317.

[4]   Colombo, F., Lentini, L., Raparelli, T., Trivella, A., and Viktorov, V., 2018, "Dynamic Characterisation of Rectangular Aerostatic Pads with Multiple Inherent Orifices," Tribology Letters, **66**(4).

[5]   Kassab, S. Z., Noureldeen, E. M., and Shawky, M. A., 1997, "Effects of Operating

Conditions and Supply Hole Diameter on the Performance of a Rectangular Aerostatic Bearing," Tribology international, **30**(7), pp. 533–545.

[6]   Charki, A., Diop, K., Champmartin, S., and Ambari, A., 2013, "Numerical Simulation and Experimental Study of Thrust Air Bearings with Multiple Orifices," International Journal of Mechanical Sciences, **72**, pp. 28–38.

[7]   Boffey, D. A., Duncan, A. E., and Dearden, J. K., 1981, "An Experimental Investigation of the Effect of Orifice Restrictor Size on the Stiffness of an Industrial Air Lubricated Thrust Bearing," Tribology International, **14**(5), pp. 287–291.

[8]   Colombo, F., Lentini, L., Raparelli, T., Trivella, A., and Viktorov, V., 2017, "Dynamic Model of a Grooved Thrust Bearing: Numerical Model and Experimental Validation," AIMETA 2017 - Proceedings of the 23rd Conference of the Italian Association of Theoretical and Applied Mechanics, pp. 506–517.

[9]   Nakamura, T., and Yoshimoto, S., 1996, "Static Tilt Characteristics of Aerostatic Rectangular Double-Pad Thrust Bearings with Compound Restrictors," Tribology international, **29**(2), pp. 145–152.

[10]   Yoshimoto, S., Tamura, J., and Nakamura, T., 1999, "Dynamic Tilt Characteristics of Aerostatic Rectangular Double-Pad Thrust Bearings with Compound Restrictors," Tribology International, **32**(12), pp. 731–738.

[11]   Witelski, T., Schwendeman, D., and Evans, P., 2008, *Analysis of Pressurized Porous Air Bearings*, 144, New Way Precision Air Bearings Inc.

[12]   Yoshimoto, S., and Kohno, K., 2001, "Static and Dynamic Characteristics of Aerostatic

Circular Porous Thrust Bearings (Effect of the Shape of the Air Supply Area)," Journal of Tribology, **123**(3), p. 501.

[13]   Kwan, Y. B. P., and Corbett, J., 1998, "Simplified Method for the Correction of Velocity Slip and Inertia Effects in Porous Aerostatic Thrust Bearings," Tribology International, **31**(12), pp. 779–786.

[14]   Kwan, Y. B. P., and Corbett, J., 1998, "Porous Aerostatic Bearings: An Updated Review," Wear, **222**(2), pp. 69–73.

[15]   Raparelli, T., Viktorov, V., Colombo, F., and Lentini, L., 2016, "Aerostatic Thrust Bearings Active Compensation: Critical Review," Precision Engineering, **44**, pp. 1–12.

[16]   Colombo, F., Lentini, L., Raparelli, T., and Viktorov, V., 2017, "Actively Compensated Aerostatic Thrust Bearing: Design, Modelling and Experimental Validation," Meccanica, pp. 1–16.

[17]   Al-Bender, F., 2009, "On the Modelling of the Dynamic Characteristics of Aerostatic Bearing Films: From Stability Analysis to Active Compensation," Precision Engineering, **33**(2), pp. 117–126.

[18]   Aguirre, G., Al-Bender, F., and Van Brussel, H., 2010, "A Multiphysics Model for Optimizing the Design of Active Aerostatic Thrust Bearings," Precision Engineering, **34**(3), pp. 507–515.

[19]   Morosi, S., and Santos, I. F., 2011, "Active Lubrication Applied to Radial Gas Journal Bearings. Part 1: Modeling," Tribology International, **44**(12), pp. 1949–1958.

[20]   Pierart, F. G., and Santos, I. F., 2016, "Active Lubrication Applied to Radial Gas Journal

Bearings. Part 2: Modelling Improvement and Experimental Validation," Tribology International, **96**, pp. 237–246.

[21]   Morosi, S., and Santos, I., 2011, "From Hybrid to Actively-Controlled Gas Lubricated Bearings : Theory and Experiment," DTU Mechanical Engineering.

[22]   Morosi, S., and Santos, I. F., 2011, "On the Modelling of Hybrid Aerostatic-Gas Journal Bearings," Proceedings of the Institution of Mechanical Engineers, Part J: Journal of Engineering Tribology, **225**(7), pp. 641–653.

[23]   Mizumoto, H., Arii, S., Kami, Y., Goto, K., Yamamoto, T., and Kawamoto, M., 1996, "Active Inherent Restrictor for Air-Bearing Spindles," Precision Engineering, **19**(2–3), pp. 141–147.

[24]   Newgard, P. M., and Kiang, R. L., 1966, "Elastic Orifices for Pressurized Gas Bearings," A S L E Transactions, **9**(3), pp. 311–317.

[25]   Blondeel, E., Snoeys, R., and Devrieze, L., 1976, "Externally Pressurized Bearings with Variable Gap Geometries," *7th International Gas Bearing Symposium*, Southampton.

[26]   Snoeys, R., and Al-Bender, F., 1987, "Development of Improved Externally Pressurized Gas Bearings," KSME Journal, **1**(1), pp. 81–88.

[27]   Bryant, M. R., Velinsky, S. A., Beachley, N. H., and Fronczak, F. J., 1986, "A Design Methodology for Obtaining Infinite Stiffness in an Aerostatic Thrust Bearing," Journal of Mechanisms, Transmissions, and Automation in Design, **108**(4), pp. 448–453.

[28]   Chen, M.-F., and Lin, Y.-T., 2002, "Dynamic Analysis of the X-Shaped Groove Aerostatic Bearings with Disk-Spring Compensator," JSME International Journal Series C, **45**, pp. 492–501.

[29]   Ghodsiyeh, D., Colombo, F., Raparelli, T., Trivella, A., and Viktorov, V., 2017, "Diaphragm Valve-Controlled Air Thrust Bearing," Tribology International, **109**, pp. 328–335.

[30]   Colombo, F., Lentini, L., Raparelli, T., Trivella, A., and Viktorov, V., 2019, "A Lumped Model for Grooved Aerostatic Pad," *Advances in Service and Industrial Robotics*, Springer International Publishing, pp. 678–686.

[31]   Colombo, F., Lentini, L., Raparelli, T., Trivella, A., and Vladimir, V., 2019, "A Nonlinear Lumped Parameter Model of an Externally Pressurized Rectangular Grooved Air Pad Bearing," *Advances in Italian Mechanism Science*, Springer, pp. 490–497.

[32]   Belforte, G., Raparelli, T., and Viktorov, V., 2002, "Modeling and Identification of Gas Journal Bearings: Self-Acting Gas Bearing Results," Journal of tribology, **124**(4), pp. 716–724.

[33]   Belforte, G., Raparelli, T., Viktorov, V., and Trivella, A., 2007, "Discharge Coefficients of Orifice-Type Restrictor for Aerostatic Bearings," Tribology International, **40**(3), pp. 512–521.

[34]   Belforte, G., Colombo, F., Raparelli, T., Trivella, A., and Viktorov, V., 2011, "Comparison between Grooved and Plane Aerostatic Thrust Bearings: Static Performance," Meccanica, **46**(3), pp. 547–555.

[35]   Colombo, F., Lentini, L., Raparelli, T., Viktorov, V., and Trivella, A., 2019, "On the Static Performance of Concave Aerostatic Pads," *Advances in Mechanism and Machine Science*, T. Uhl, ed., Springer International Publishing, pp. 3919–3928.